The following resources related to this article are available online at
www.sciencemag.org (this information is current as of January 15, 2008):

Updated information and services, including high-resolution figures, can be found in the online
version of this article at:
http://www.sciencemag.org/cgi/content/full/318/5854/1258

Supporting Online Material can be found at:
http://www.sciencemag.org/cgi/content/full/318/5854/1258/DC2

A list of selected additional articles on the Science Web sites **related to this article** can be
found at:
http://www.sciencemag.org/cgi/content/full/318/5854/1258#related-content

This article **cites 64 articles**, 29 of which can be accessed for free:
http://www.sciencemag.org/cgi/content/full/318/5854/1258#otherarticles

This article has been **cited by** 2 article(s) on the ISI Web of Science.

This article has been **cited by** 2 articles hosted by HighWire Press; see:
http://www.sciencemag.org/cgi/content/full/318/5854/1258#otherarticles

This article appears in the following **subject collections**:
Biochemistry
http://www.sciencemag.org/cgi/collection/biochem

Information about obtaining **reprints** of this article or about obtaining **permission to reproduce**
this article in whole or in part can be found at:
http://www.sciencemag.org/about/permissions.dtl

High-Resolution Crystal Structure of an Engineered Human β₂-Adrenergic G Protein–Coupled Receptor
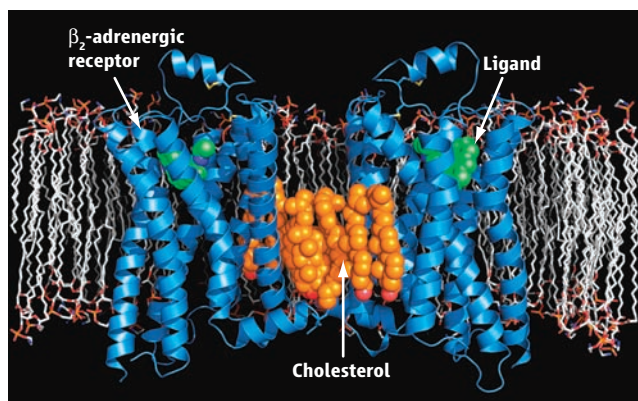
Vadim Cherezov,[1]* Daniel M. Rosenbaum,[2]* Michael A. Hanson,[1]
Søren G. F. Rasmussen,[2] Foon Sun Thian,[2] Tong Sun Kobilka,[2] Hee-Jung Choi,[2,3]
Peter Kuhn,[4] William I. Weis,[2,3] Brian K. Kobilka,[2]† Raymond C. Stevens[1]†

AUTHORS' SUMMARY

The largest family of integral membrane proteins coded by the human genome comprises G protein–coupled receptors (GPCRs), with almost 1000 members (1, 2). These receptors communicate signals across cell membranes in response to an astonishing variety of extracellular stimuli—light, proteins, peptides, small molecules, hormones, and ions. Once activated, GPCRs trigger a cascade of responses inside the cell, primarily through interactions with their G protein partners, three-subunit regulators that are switched on and off by binding guanosine triphosphate (GTP) (thus accounting for their name). In addition, these receptors have been found to activate other, G protein–independent, signaling pathways. Their combined effects yield an amazingly diverse network of signals that must be exquisitely coordinated to ensure proper cellular function (3, 4).

Structure of the human β₂-adrenergic receptor (blue) embedded in a lipid membrane and bound to a diffusible ligand (green), with cholesterol and palmitic acid (orange) between the two receptor molecules.

Although drugs that act on GPCRs command more than 50% of the current market for human therapeutics, with annual revenues in excess of $40 billion, these drugs interact with only a fraction of the available receptors. Because of the importance of this protein family, there is an ongoing search for new drugs that act on GPCRs and that combine potent efficacy with high specificity. Of particular interest are the class A adrenergic receptors that respond to the hormones adrenaline and noradrenaline. These are the targets of current cardiac and asthma drugs that often have undesirable side effects. In addition, improved asthma drugs are needed in developing countries where the population and pollution levels are rapidly rising, along with the incidence of asthma. Structures of GPCRs can guide the development of more specific drugs and can be combined with traditional chemical screening methods to improve and accelerate drug discovery.

For protein structures to effectively guide drug design, it is critically important to maximize the available detail, as low-resolution structures can be ambiguous at best and misleading at worst. However, it remains a formidable challenge to obtain high-resolution structural data for membrane proteins. To accomplish this, we engineered the β₂-adrenergic receptor to include lysozyme in place of one of the intracellular loops, which reduced conformational heterogeneity and facilitated crystal nucleation [see (5)]. Crystals were grown in a cholesterol-doped lipidic cubic phase that stabilized the receptor in a more natural membrane-like environment. We used a robot to set up more than 15,000 trials to optimize crystal growth in the extremely viscous lipidic cubic mesophase. We then evaluated the micrometer-size transparent crystals with a 10-μm x-ray beam. Our resulting 2.4 Å crystal structure of the human β₂-adrenergic receptor successfully provides high-resolution detail.

The crystal structure of this important human membrane receptor reveals the details of its interactions with a diffusible ligand (the partial inverse agonist carazolol). In examining the structure, one can begin to appreciate the amazing structural plasticity of the GPCRs and how this allows them to recognize such a wide range of ligands critical for function within the human body. The ligand-binding site of the β₂-adrenergic receptor is located in a position similar to that of the covalently bound ligand of rhodopsin, the light-absorbing, G protein–coupled receptor responsible for human vision. Key differences from rhodopsin are also observed, particularly in several of the kinked transmembrane helices and in the second extracellular loop, which in the β₂-adrenergic receptor contains an unusual pair of disulfide bonds and an extra helix. This loop and the absence of structure in the N-terminal region of the receptor may be important for ligand binding.

Although this structure of a GPCR that recognizes a diffusible ligand furthers understanding of signal transduction and should facilitate the design of new drugs with fewer side effects, the structure alone cannot fully explain how ligand binding on the outside surface of a cell triggers internal signaling pathways. This will require characterization of how the receptor changes its conformation as it is activated. Follow-up structures or receptors bound to other ligands will be required to understand the different conformational states and how they transduce signals. It is possible that the active state will only be understood when a structure is obtained for a GPCR–G protein signaling complex with an agonist bound to the receptor. In addition, structural and complementary biophysical techniques (e.g., nuclear magnetic resonance) will help to resolve other key biological questions, including the effects of homodimerization or heterodimerization of the receptor, the nature of class B and C GPCR structures, and elucidation of cholesterol's role in GPCR function.

Summary References
1. S. Takeda, S. Kadowaki, T. Haga, H. Takaesu, S. Mitaku, *FEBS Lett.* **520**, 97 (2002).
2. R. Fredriksson, M. C. Lagerstrom, L. G. Lundin, H. B. Schioth, *Mol. Pharmacol.* **63**, 1256 (2003).
3. K. L. Pierce, R. T. Premont, R. J. Lefkowitz, *Nat. Rev. Mol. Cell Biol.* **3**, 639 (2002).
4. R. J. Lefkowitz, S. K. Shenoy, *Science* **308**, 512 (2005).
5. D. M. Rosenbaum *et al.*, *Science* **318**, 1266 (2007); published online 25 October 2007 (10.1126/science.1150609).

FULL-LENGTH ARTICLE

Heterotrimeric guanine nucleotide–binding protein (G protein)–coupled receptors constitute the largest family of eukaryotic signal transduction proteins that communicate across the membrane. We report the crystal structure of a human β_2-adrenergic receptor–T4 lysozyme fusion protein bound to the partial inverse agonist carazolol at 2.4 angstrom resolution. The structure provides a high-resolution view of a human G protein–coupled receptor bound to a diffusible ligand. Ligand-binding site accessibility is enabled by the second extracellular loop, which is held out of the binding cavity by a pair of closely spaced disulfide bridges and a short helical segment within the loop. Cholesterol, a necessary component for crystallization, mediates an intriguing parallel association of receptor molecules in the crystal lattice. Although the location of carazolol in the β_2-adrenergic receptor is very similar to that of retinal in rhodopsin, structural differences in the ligand-binding site and other regions highlight the challenges in using rhodopsin as a template model for this large receptor family.

G protein–coupled receptors (GPCRs) constitute the largest integral membrane protein family in the human genome, with almost 1000 members (*1*, *2*). GPCRs are major contributors to the information flow into cells and, as such, are associated with a multitude of diseases that make members of this family important pharmacological targets (*3–6*).

GPCRs have been grouped into five classes (*2*) on the basis of sequence conservation, with class A being the largest and most studied. Class A receptors are further divided into groups associated with particular ligand specificity, such as the opsin, amine, peptide, cannabinoid, and olfactory receptors. The adrenergic receptors in the amine group are among the most thoroughly investigated class A GPCRs (*7–12*) and consist of two main subfamilies, α and β, which differ in tissue localization and ligand specificity as well as in G protein coupling and downstream effector mechanisms (*13*). Genetic modifications of adrenergic receptors are associated with diseases as diverse as asthma, hypertension, and heart failure (*14*). β_2-Adrenergic receptors (β_2ARs) reside predominantly in smooth muscle throughout the body, and β_2AR agonists are used in the treatment of asthma and preterm labor (*15–17*).

Despite extensive efforts, structural information for only one member of the eukaryotic GPCR family, bovine rhodopsin, is available to date (*18–21*). Rhodopsin is unusual in that it is highly abundant from natural sources and is structurally stabilized by the covalently bound ligand 11-*cis*-retinal, which maintains the receptor in a dark-adapted, nonsignaling con-

formation. In contrast, all other GPCRs are activated by diffusible ligands and are expressed at relatively low levels in native tissues. These receptors are structurally more flexible and equilibrate among multiple conformational states, some of which are prone to

instability (*22*). Although the structure determination of rhodopsin was important, many questions remain concerning the conformational changes between different activation states for each receptor, as well as the structural differences among receptors that accommodate the very large diversity of ligands. What structural features enable GPCRs to recognize and bind diffusible ligands? How structurally conserved are the class A GPCRs, and what is the importance of their similarities and differences?

To address these questions, we modified the human β_2AR to facilitate the growth of diffraction-quality crystals by inserting T4 lysozyme (T4L) in place of the third intracellular loop (β_2AR-T4L) and solved the three-dimensional crystal structure in the presence of a partial inverse agonist, carazolol (2-propanol, 1-9*H*-carbazol-4-yloxy)-3-[(1-methylethyl)amino]) at 2.4 Å resolution (*23*, *24*). We provide a comprehensive analysis of the crystal packing and intramolecular contacts between the β_2AR and

[1]Department of Molecular Biology, Scripps Research Institute, La Jolla, CA 92037, USA. [2]Department of Molecular and Cellular Physiology, Stanford University School of Medicine, Stanford, CA 94305, USA. [3]Department of Structural Biology, Stanford University School of Medicine, Stanford, CA 94305, USA. [4]Department of Cell Biology, Scripps Research Institute, La Jolla, CA 92037, USA.

*These authors contributed equally to this work.

†To whom correspondence should be addressed. E-mail: stevens@scripps.edu (R.C.S.); kobilka@stanford.edu (B.K.K.)

Table 1. Data collection and refinement statistics.

	β_2AR-T4L
*Data collection (APS GM/CA CAT 23ID-B, 10-μm beam)**	
Space group	*C*2
Cell dimensions	
a, *b*, *c* (Å)	106.3, 169.2, 40.2
β (°)	105.62
Number of reflections processed	245,571
Number of unique reflections	26,574
Resolution (Å)	50 to 2.4 (2.5 to 2.4)
R_{sym}†	12.7 (67.8)
Mean $I/\sigma(I)$	9.6 (2.2)
Completeness (%)	99.5 (99.1)
Redundancy	9.4 (4.8)
*Refinement**	
Resolution (Å)	20 to 2.4 (2.46 to 2.4)
Number of reflections (test set)	25,247 (1310)
R_{work} / R_{free}	19.8 (27.0) / 23.2 (30.1)
Number of atoms	3805
Protein	3544
Ions, lipids, ligand, and other	213
Water	48
Overall *B* values (Å²)	82
β_2AR	77
T4 lysozyme	75
Carazolol	55
Lipid	100
RMSD	
Bond lengths (Å)	0.013
Bond angles (°)	1.5
Ramachandran plot statistics (%) (excluding Gly, Pro):	
Most favored regions	94.8
Additionally allowed regions	5.0
Generously allowed regions	0.2
Disallowed regions	0

*Highest-resolution shell is shown in parentheses.   †$R_{sym} = \Sigma_{hkl} |I(hkl) - \langle I(hkl)\rangle|/\Sigma_{hkl}(hkl)$, where $\langle I(hkl)\rangle$ is the mean of the symmetry-equivalent reflections of $I(hkl)$.

T4L to identify potential receptor-perturbing interactions. The overall receptor topology and the ligand-binding pocket are described, as are the main similarities and differences between β_2AR-T4L and rhodopsin.

Structure determination. The engineering, functional properties, expression, and purification of crystallization-grade β_2AR-T4L protein are described fully in the companion paper (24, 25). Briefly, β_2AR-T4L was expressed in Sf9 insect cells, solubilized in 1% dodecylmaltoside, and purified by sequential antibody and ligand affinity chromatography. Following the reported success with microbial rhodopsins in lipidic cubic phase (LCP) (26), we were able to produce crystals of β_2AR-T4L that diffracted to a resolution of 2.2 Å with a modified LCP procedure, and we solved and refined the structure at 2.4 Å resolution (27). Relative to crystallization in detergents, LCP provides a more native, lipid environment for crystallization, as well as a confinement of protein molecules to two-dimensional membrane sheets that may facilitate the crystallization process through the formation of type I packing interactions (28–30). In agreement with prior biological evidence that cholesterol improves β_2AR stability (31) and may mediate receptor-receptor interactions, crystals were grown from a cholesterol-doped monoolein cubic phase. An automated, nanovolume LCP crystallization protocol (32) substantially reduced the time and amount of protein required for the exhaustive, multidimensional optimization trials needed to arrive at these conditions. Crystals of β_2AR-T4L were also obtained in lipid bicelles, but they did not diffract as well as those obtained in LCP (27).

Diffraction data for β_2AR-T4L were measured to a resolution of 2.4 Å from a total of 27 microcrystals (average size 30 μm by 15 μm by 5 μm) using a high-intensity, highly parallel minibeam with a diameter of 10 μm at the GM/CA-CAT beamline of the Advanced Photon Source, Argonne National Laboratory (33). Phase information was obtained by molecular replacement using both T4L (PDB ID code 2LZM) and a polyalanine model of the transmembrane regions of rhodopsin (PDB ID code 1U19) as search models. Additional crystallization, data collection, processing, and refinement statistics are reported in Table 1 and discussed in (27).

Overall receptor topology. The final model of β_2AR-T4L includes 442 amino acids. The model also includes a palmitic acid covalently bound to Cys341 and an acetamide molecule bound to Cys265[6.27] (residues are designated by their position within the β_2AR sequence; where applicable, their Ballesteros-Weinstein designations appear as superscripts) (34, 35), as well as one carazolol molecule, three cholesterol molecules, two sulfate ions, and two butanediol molecules that interact

with β_2AR. There are also four sulfate ions, a putative disaccharide (modeled as maltose), and a molecule of polyethylene glycol 400 bound to T4L. For β_2AR, excellent electron density was observed for residues 29 to 342, including the ligand carazolol and the two disulfide bonds Cys106[3.25]-Cys191[5.30] and Cys184[4.76]-Cys190[5.29]. The palmitic acid at Cys341 was clearly visible in $F_{obs} - F_{calc}$ omit maps; however, the quality of the electron density was lower than for the rest of the receptor. The N terminus (residues 1 to 28) and the majority of the C terminus (residues 343 to 365) were disordered and not visible in the structure.

The β_2AR has a fold composed of seven transmembrane helices forming a helical bundle (Fig. 1A). The residues that make up the helices (I to VII) in β_2AR are as follows: helix I, positions 29[1.28] to 60[1.59]; helix II, positions 67[2.38] to 96[2.67]; helix III, positions 103[3.22] to 136[3.55]; helix IV, positions 147[4.39] to 171[4.63]; helix V, positions 197[5.36] to 229[5.68]; helix VI, positions 267[6.29] to 298[6.60]; and helix VII, positions 305[7.32] to 328[7.55]. The residues forming the intracellular loops (ICLs) and extracellular loops (ECLs) of β_2AR are as follows: ICL1, positions 61[1.60] to 66[2.37]; ECL1, positions 97[2.68] to 102[3.21]; ICL2, positions 137[3.56] to 146[4.38]; ECL2, positions
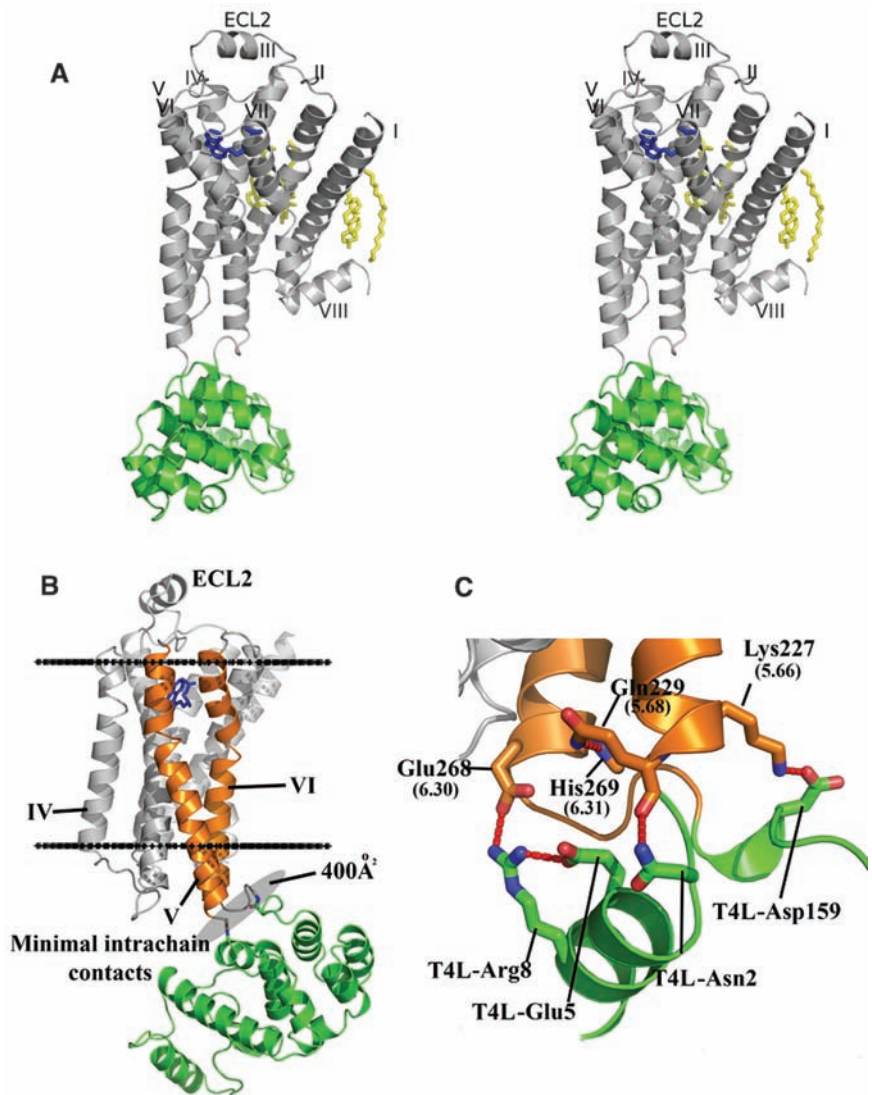
Fig. 1. Overall fold of the β_2AR-T4L fusion with its predicted orientation in the plasma membrane and key intramolecular interactions. (**A**) Stereoview of the overall fold of β_2AR-T4L. The receptor and T4L are colored gray and green, respectively. Carazolol is shown in blue; the lipid molecules bound to the receptor are in yellow. (**B**) The receptor is aligned to a rhodopsin model that was positioned in a lipid membrane (boundaries indicated by horizontal black lines) as found in the Orientations of Proteins in Membranes database (74). T4L is fused internally into the third intracellular loop of β_2AR and maintains minimal intramolecular packing interactions by tilting away from the receptor. (**C**) Specific intramolecular interactions between β_2AR and T4L.

$172^{4.64}$ to $196^{5.35}$; ICL3, positions $230^{5.69}$ to $266^{6.28}$ (residues 231 to 262 are replaced by T4L residues 2 to 161); and ECL3, positions $299^{6.61}$ to $304^{7.31}$. Helices II, V, VI, and VII each have a proline-induced kink at conserved positions along the span of the transmembrane segments. These kinks are thought to enable the structural rearrangements required for activation of G protein effectors (36). In addition to the seven membrane-spanning helices, β_2AR has two other helical segments: helix VIII, which is believed to be common to all rhodopsin-like GPCRs (37), and an unexpected, short helical segment in the middle of ECL2, which is not present in rhodopsin and was not predicted by computational secondary structure analysis (Fig. 1A).

In the β_2AR-T4L construct, T4L is fused to the truncated cytoplasmic ends of helices V and VI. In the crystal structure, the T4L moiety is tilted slightly away from the center axis of β_2AR drawn normal to the membrane (Fig. 1B). As a result, interactions between T4L and β_2AR are minimal, with only 400 Å^2 of surface area buried between them. The intramolecular contacts between T4L and β_2AR include salt bridges between the side chains of T4L-Asp^{159} and the side-chain amine of β_2AR-Lys227$^{5.66}$ (distance 3.4 Å) and between the guanidinium group of T4L-Arg^8 and the side-chain carboxyl of β_2AR-Glu268$^{6.30}$ on helix VI (distance 3.2 Å) (Fig. 1C and table S2). The latter interaction is noteworthy, because in rhodopsin Glu$^{6.30}$ forms an ionic bond with Arg$^{3.50}$ of the conserved Asp-(Glu)-Arg-Tyr motif (18). This interaction is postulated to be important for maintaining rhodopsin in the inactive state, but the charged groups of the two residues [Arg131$^{3.50}$ (NH1) and Glu268$^{6.30}$ (OE1)] are 10 Å apart in the β_2AR-T4L structure. Possible functional implications of this disruption are discussed in (24). The remainder of the lysozyme molecule provides important crystal-packing interactions but does not appear to influence the receptor structure.

Crystal-packing interactions. The β_2AR-T4L protein is packed in a C-centered monoclinic lattice with one molecule per asymmetric unit (Fig. 2A). As observed in all previous lipidic mesophase–grown crystals (38), the β_2AR-T4L crystals adopt type I packing (39), featuring a multilayered arrangement in accordance with a proposed crystallization mechanism (28, 40). Within each layer, protein molecules form arrays of parallel, symmetry-related dimers. There are four distinct crystal-packing interactions within each layer, three of which are mediated by T4L. The fourth interaction in the array is between two receptor molecules related by a crystallographic two-fold rotation axis. This is the sole interaction between symmetry-related receptors and is mediated primarily by ordered lipids consisting of six cholesterol and two palmitic acid molecules, the latter being covalently attached to Cys^{341} in the C-terminal portion of the receptor (41) (Fig. 2B). These eight lipid molecules form a two-fold symmetric sheet between receptors. The only direct receptor-receptor contact involves a 2.7 Å pair of ionic interactions between the charged amine group of Lys60$^{1.59}$ in helix I and the carboxylate of Glu^{338} in helix VIII from the symmetry-related receptor. Remarkably, of the 515 Å^2 buried at the receptor symmetry interface, 73% of the crystal contact surface area is mediated by ordered lipid, whereas only 27% is contributed by protein-protein contacts. The stacking interactions between layers are formed between T4L and extracellular loops ECL2 and ECL3 of the receptor (Fig. 2A). Because of the small size of ECL3 and the rigid architecture of ECL2, it is unlikely that these contacts affect the orientation of these loops.

Lipid-mediated receptor association. Many GPCRs including β_2AR are thought to exist as dimers in the plasma membrane, although the location of the dimer interface and the functional importance of dimerization are not clear (42). The observation of ordered lipids in the helix I–helix VIII interface between two symmetry-related molecules makes it tempting to speculate on the physiological relevance of this association (43–45). Associations between the equivalent regions of rhodopsin have been found in crystal structures (21, 46) (Fig. 2C). On the other hand, studies in native membranes suggest that helix VI may form the dimer interface for the β_2AR (47), and helix IV may form the dimer interface for the closely related D_2 dopamine receptor (48).

Although the role of cholesterol in promoting β_2AR association is speculative, its role in the physiologic function of β_2AR is well documented. Depletion of cholesterol from the membranes of neonatal cardiac myocytes alters the signaling behavior of endogenous β_2AR (49). In untreated cells, activation of β_2AR results in sequential coupling to the G
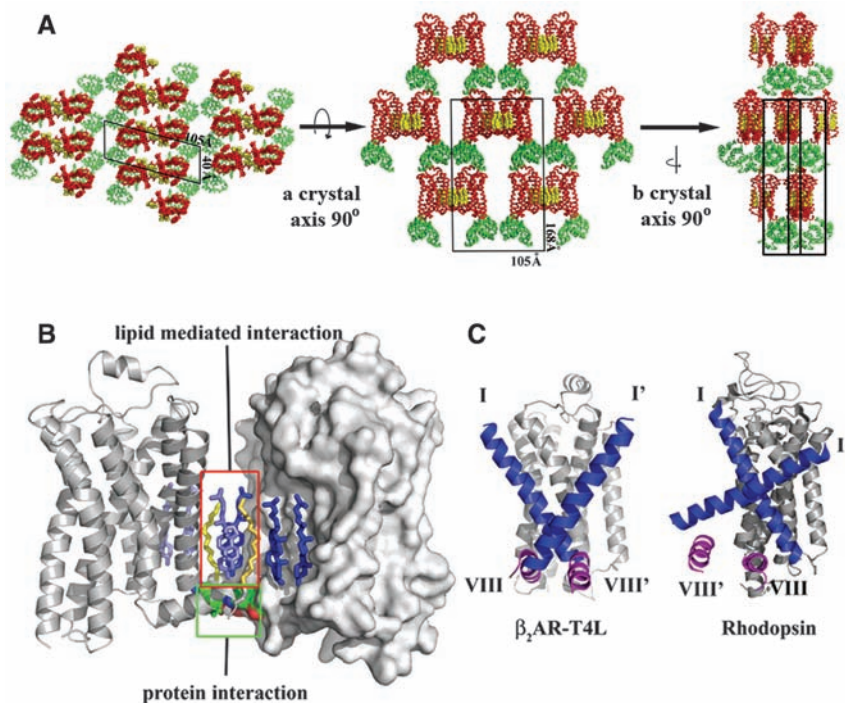
Fig. 2. Crystal-packing interactions in the lipidic mesophase–crystallized β_2AR-T4L. (**A**) There are four main contact areas, two of which are mediated by T4L in the plane of the membrane with itself through a two-fold symmetry axis and translation. The third interaction is normal to the membrane plane between T4L and lumen-exposed loops of β_2AR. The fourth interaction is generated by the two-fold symmetry axis, packing one receptor to another in the plane of the membrane. (**B**) The receptor crystal-packing interface is composed mainly of lipids, with two cholesterol molecules and two palmitic acid molecules forming the majority of the interactions. A network of ionic charge interactions exists on the cytoplasmic end of the interface, forming the only interreceptor protein contacts. (**C**) Comparison between β_2AR-T4L and rhodopsin (PDB ID code 2I35) parallel receptor association interface. Helices I (blue) and VIII (magenta) are highlighted in both structures. Only one monomer is shown for each receptor representation, along with helices I′ and VIII′ only from the opposing symmetry-related molecule. The rhodopsin interface is twisted relative to β_2AR-T4L, resulting in a substantial offset from the parallel orientation required for a physiological dimer interface. β_2AR-T4L–associated monomers are in a highly parallel orientation.

proteins G_s and G_i, producing a biphasic effect on myocyte contraction rate. Upon depletion of cholesterol, the β_2AR couples more strongly to G_s. This effect may be due to a role of cholesterol in regulating interactions between the β_2AR and G proteins, or possibly to the effect of cholesterol on β_2AR dimerization. The β_2AR couples efficiently to G_s as a monomer (50), so it is possible that cholesterol-mediated association (dimerization) reduces the efficiency of β_2AR coupling to G_s. The effects of cholesterol depletion on β_2AR signaling may also be a secondary effect of altering subcellular signaling compartments. There is evidence that cells may concentrate signaling molecules, such as GPCRs and their cognate G proteins, by way of membrane microdomains or compartments such as caveolae (51). This compartmentalization may be a major regulator of receptor-effector coupling. Thus, the importance of cholesterol in forming the observed crystallographic association is consistent with its role in β_2AR signaling. Additional experiments will be required to determine whether the association of monomers observed in the crystal is relevant to β_2AR packing within membrane microdomains.

Electrostatic charge distribution. Electrostatic charge distribution was calculated using the program APBS (52) and mapped onto a molecular surface representation of β_2AR. The analysis reveals three polarized areas within the molecule (Fig. 3A). First, the cytoplasmic face of the receptor is involved in G protein interaction and carries a net positive charge even in the absence of ICL3, which also has a predicted overall positive charge (Fig. 3B). The second site is an electrostatically negative region located within the membrane between helices III, IV, and V potentially exposed to the lipid alkyl chains, which is unexpected because the burial of charge within the plasma membrane is thermodynamically unfavorable. A Glu residue at position 122$^{3.41}$ may partially account for the observed charge distribution. Finally, the binding-site cleft is negatively charged and exposed to solvent by an unusual ECL2 architecture and a lack of N-terminal interactions. This negative charge may facilitate ligand binding through electrostatic funneling of positively charged catecholamines (Fig. 3B).

Extracellular region. The ECLs and N termini of GPCRs, together with the extracellular halves of the transmembrane helices, are believed to define the ligand-binding site of each receptor (43). Therefore, the ECLs may play an important role in the overall pharmacology of any particular receptor. In general, small-molecule ligands are thought to bind deeper within the space created by the transmembrane domain helices, whereas larger ligands such as peptides bind closer to the membrane surface near the ECLs (53, 54). Mutagenesis studies suggest that the β_2AR

binds its ligand deep within the transmembrane helix bundle, which may be related to the observation that the extracellular regions have a rather simple structure with short loops connecting transmembrane helices II and III with helices VI and VII (Fig. 4A). ECL2, which links helices IV and V, has a somewhat more extensive architecture that is unanticipated. In contrast to the buried β-sheet structure of this loop in rhodopsin (Fig. 4B), ECL2 in β_2AR is more exposed to the solvent and contains an extra helical segment. Additional-
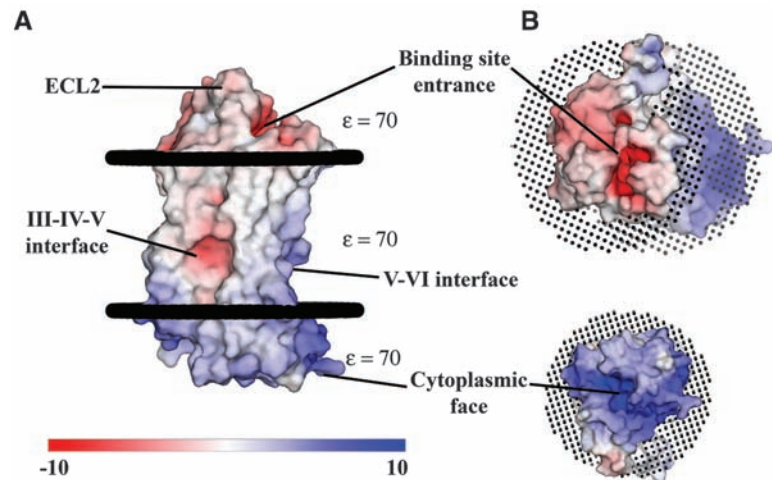
Fig. 3. Surface representation of β_2AR colored by calculated charge from red (-10 k_bT/e_c) to blue ($+10$ k_bT/e_c) using a dielectric constant of 70. (**A**) Three main areas of interest are indicated. The binding-site cleft is negatively charged, as is a groove between helices III, IV, and V. The third region is an overall positive charge in the region of the ionic lock and Asp-Arg-Tyr motif on the cytoplasmic face. The overall result is a highly polarized molecule that may use its negative charge to facilitate binding of catecholamine ligands. The presence of a negative charge in the groove between helices III, IV, and V is unexpected, as it is in the middle of the lipid membrane. This charge may be partially derived from the presence of an unpaired glutamate at position 122$^{3.41}$. The effective charge in this region is likely greater than shown here because of its location in the low-dielectric environment of the lipid membrane. (**B**) View rotated 90° from (A), showing the negatively charged binding-site cleft (top) and the positively charged cytoplasmic face (bottom). Poisson-Boltzmann electrostatics were calculated using APBS (52) as implemented in PyMOL (75). PyMOL was used exclusively in the preparation of all figures.
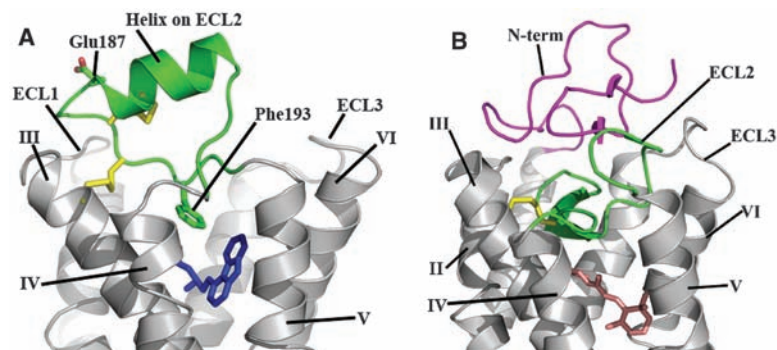
Fig. 4. Comparison of the extracellular sides of β_2AR-T4L and rhodopsin. (**A**) The N terminus is missing from the experimental density in the β_2AR-T4L structure and is not shown. ECL2 is shown in green and contains a short α helix and two disulfide bonds (yellow). The intraloop disulfide bond constrains the tip of ECL2, which interacts with ECL1. The second disulfide bond links ECL2 with helix III. There is one interaction between ECL2 and carazolol (blue) through Phe193$^{5.32}$. The entire loop is held out of the ligand-binding site by a combination of the rigid helical segment and the two disulfide bonds. (**B**) In contrast, ECL2 (green) in rhodopsin assumes a lower position in the structure that occludes direct access to the retinal-binding site and forms a small β sheet in combination with the N-terminal region (magenta) directly above the bound retinal (pink).

ly, there is an intraloop disulfide bond between Cys184[4.76] and Cys190[5.29] that may help stabilize the more exposed ECL2. A second disulfide bond between Cys191[5.30] and Cys106[3.25] in helix III effectively ties ECL2 to the transmembrane core (55). The distal portion of ECL2 makes close contacts with ECL1 and contains a glycosylation site at Asn187[5.26] (56), which may serve to mask a grouping of aromatic residues on ECL1; in this construct, Asn187[5.26] has been mutated to Glu to aid in crystallization.

Electron density corresponding to the N terminus was not apparent in the maps, and therefore residues 1 to 28 are not included in the model. This disorder contrasts with rhodopsin, in which the N terminus interacts extensively with the ECLs, forming a small four-strand β sheet in conjunction with ECL2. This sheet structure forms a cap that effectively isolates the retinal-binding site in a hydrophobic pocket (Fig. 4B). The lack of interactions between the N terminus of β2AR and ECL2 further enables diffusible ligand access to the binding site. However, a completely disordered N terminus may be an artifact induced by the presence of the N-terminal Flag tag, which carries an overall positive charge and may disrupt N-terminal interactions.

The short helical region on ECL2 adds a rigid structural element that, along with the two disulfide bonds, constrains the loop to a small range of conformations and helps stabilize the receptor by linking three transmembrane helices (Fig. 4A). This rigid conformation may help to stabilize the core of the receptor and lock ECL2 in a conformation that does not hinder access to the binding pocket.

Ligand-binding site and comparison to rhodopsin. Carazolol is a partial inverse agonist that binds with picomolar affinity to β2AR-T4L, producing a reduction of the basal activity of the receptor (57). The crystal structure reveals extensive interactions between the receptor and carazolol that position the carbazole moiety adjacent to Phe289[6.51], Phe290[6.52], and Trp286[6.48] (Fig. 5A, fig. S1, and table S3). In contrast, 11-cis-retinal is a full inverse agonist covalently bound to rhodopsin, which suppresses all activity toward transducin (58). Carazolol and retinal occupy similar spaces in their respective receptors, with substantial overlap of the nonaromatic regions of carazolol. However, the β-ionone ring of retinal extends deep into the binding pocket of rhodopsin and contacts residues on helices V and VI, where it is sandwiched between Phe212[5.47] and Tyr268[6.51] and interacts with the highly conserved Trp265[6.48] (Fig. 5B). It has been proposed that changes in the rotamer of Trp265[6.48] occur upon activation of rhodopsin and related family members, and that these changes constitute the "toggle switch" for receptor activation (59). Accordingly, the interactions between 11-cis-retinal and Trp265[6.48] are likely to contribute to the absence of basal activity in rhodopsin. Carazolol does not interact directly with the toggle switch on helix VI; however, it lowers the basal activity of the receptor, and may do so by interacting with Phe289[6.51] and Phe290[6.52], which form an extended aromatic network surrounding the highly conserved Trp286[6.48]. As a result, Trp286[6.48] adopts the rotamer associated with the inactive state. Thus, the steric constraints imposed by Phe290[6.52] appear to

structurally mimic the interaction of the β-ionone ring of retinal with the conserved Trp286[6.48] and Phe212[5.47] on rhodopsin (60) (Fig. 5C).

Structural alignment and helix bundle reorganization. It has long been thought that class A GPCRs share a similar architecture as a result of their predicted seven-transmembrane helical bundles and sequence conservation within the membrane-spanning regions (61). To learn more about the structural similarities and differences in class A GPCRs, we aligned the structure of β2AR-T4L to highest-resolution structure of rhodopsin (PDB ID code 1U19). We used difference distance matrices to select nondivergent areas between the two structures that align to reveal the differences in helix orientation between β2AR-T4L and rhodopsin (62).

Relative to rhodopsin, the following helical shifts are seen in β2AR-T4L: The extracellular portions of helices I and III angle away from the center of the receptor, helix IV is translated away from the center of the receptor, helix V is translated closer to the center of the receptor, and helix VI angles away from the receptor on the cytoplasmic end (Fig. 6). The largest difference is in helix I, which lacks a proline-induced kink found in rhodopsin and is comparatively straight. The angle between the rhodopsin and β2AR positions of helix I is about 18° with a shift of 7 Å at the apex on the extracellular face. This structural difference may arise from the need for an accessible binding site in β2AR, which is provided in part by a lack of interactions between the N terminus and extracellular loop segments. In contrast, the N-terminal

Fig. 5. Ligand-binding characterization and comparison to rhodopsin. (**A**) View looking down on the plane of the membrane from the extracellular surface, showing a detailed representation of the carazolol-binding site in β2AR-T4L. Carazolol is shown as sticks with carbon atoms colored yellow. β2AR-T4L residues contributing to carazolol binding are shown in green and labeled. Electron density is contoured at 5σ from an $F_{obs} - F_{calc}$ omit map calculated without the contribution of carazolol. Abbreviations: D, Asp; F, Phe; N, Asn; S, Ser; W, Trp; Y, Tyr. (**B**) Binding orientation comparison between 11-cis-retinal in rhodopsin and carazolol in β2AR-T4L. Van der Waals surfaces for carazolol and retinal are represented as dots to accentuate the close-packing interactions. Retinal in the 11-cis conformation (pink) binds deep in the active site of rhodopsin as compared to carazolol (blue), packing its β-ionone ring between Tyr268[6.51] and Phe212[5.47] (cyan) and blocking movement of Trp265[6.48] (magenta) into the space. The β-ionone ring of all-trans-retinal in activated rhodopsin would not block Trp265[6.48] from rotating into the space, allowing a rotameric shift into its proposed active form. (**C**) Four residues are involved in the toggle switch mechanism of β2AR-T4L. Phe290[6.52] (magenta) is sandwiched between Phe208[5.47] (tan) and Phe289[6.51] (tan), forming a ring-face aromatic interaction. Like rhodopsin, an activation step is thought to occur by a rotameric change of Trp286[6.48] (magenta), which would displace Phe290[6.52]. Carazolol is shown to interact extensively with the sandwich motif; however, few interactions are seen with Trp286[6.48]. The 6.52 position in β2AR-T4L is occupied by Phe290[6.52], as opposed to Ala269[6.52] in rhodopsin, where the β-ionone ring replaces an aromatic protein side chain in forming the sandwich interactions. The aromatic character of the sandwich is otherwise maintained by Phe289[6.51] and Phe208[5.47] in β2AR-T4L.
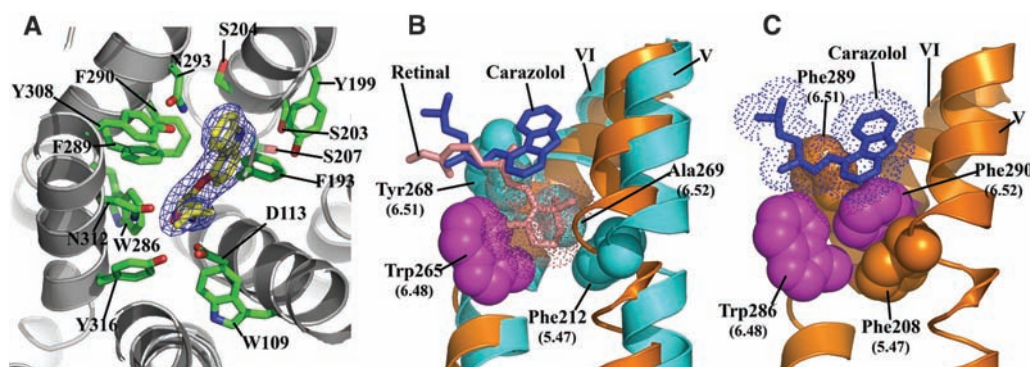
region in rhodopsin occludes the retinal-binding site through extensive interactions with the extracellular loops (Fig. 4B). Helix V of β_2AR is closer to the binding pocket by about 3.5 Å on average, and its lumenal end is angled more toward helix VI. Helix IV of β_2AR is farther from the binding site, possibly to remove steric clashes resulting from the modified position of helix V (Fig. 6, B and C). Helix III pivots farther from the binding site about a fulcrum located close to the cytoplasmic end (Fig. 6C). The angle formed between rhodopsin helix III and β_2AR helix III is about 7°, yielding a 4 Å displacement out of the binding pocket at the cytoplasmic end of the helix. Relative to rhodopsin, helix VI of β_2AR is positioned farther from the

center of the receptor at the cytoplasmic end; this is caused by a slight difference in the angle about the proline-induced kink in the helix (Fig. 6C).

The ligand-binding pocket is formed by both structurally conserved and divergent helices, in the context of their positions in rhodopsin (Fig. 6D). Helices III and V are two of the most conformationally shifted helices and contain the canonical catecholamine-binding residues associated with activation of the adrenergic family of receptors (63–65). The comparison with rhodopsin suggests that the structurally conserved helices provide a common core present throughout the class A GPCRs, whereas the variable helices confer binding-site plasticity with a resulting archi-

tecture capable of binding a large spectrum of ligands.

Comparison to rhodopsin-based GPCR models. Since the determination of the inactive dark-state rhodopsin structure (18), a number of homology models of other class A GPCRs have been reported (66–70). Typically, homology models start by alignment of so-called fingerprint motifs that are common among the family. These fingerprint motifs are extrapolated to assign coordinates for the entire helical bundle. Loop regions are either ignored or modeled on the basis of databases of loop conformations, depending on the application (66). A number of models exist for β_2AR, some of which have been improved upon with supporting biochemical data (66, 70–73). When compared to the β_2AR structure reported here, however, all of these models were more similar to rhodopsin, as were models for other receptors (e.g., dopamine, muscarinic, and chemokine) (27). This is not entirely surprising but highlights a general shortcoming in homology models generated from a single structural template. The structural divergence between β_2AR and rhodopsin would be quite difficult to predict accurately using only rhodopsin as a template. The addition of a second class A GPCR structure should make it possible to correlate the sequence differences between rhodopsin and β_2AR with the observed structural differences, enabling extrapolation to other class A GPCRs. Highlighting interactions that constrain class A receptors into each of the two observed states will allow a more comprehensive analysis of structural divergence and should result in more accurate models. Furthermore, evidence provided in (24) indicates that β_2AR-T4L may not be in a completely inactive conformation like rhodopsin, providing an alternative signaling state on which to base homology models that will be more relevant for virtual ligand screening and structure-based drug design (66, 73). The addition of further structural templates and conformational states to the pool of information on GPCRs should pave the way to a new generation of more potent therapeutics targeting this expansive receptor family and enhance our understanding of the signaling properties within their associated pathways.
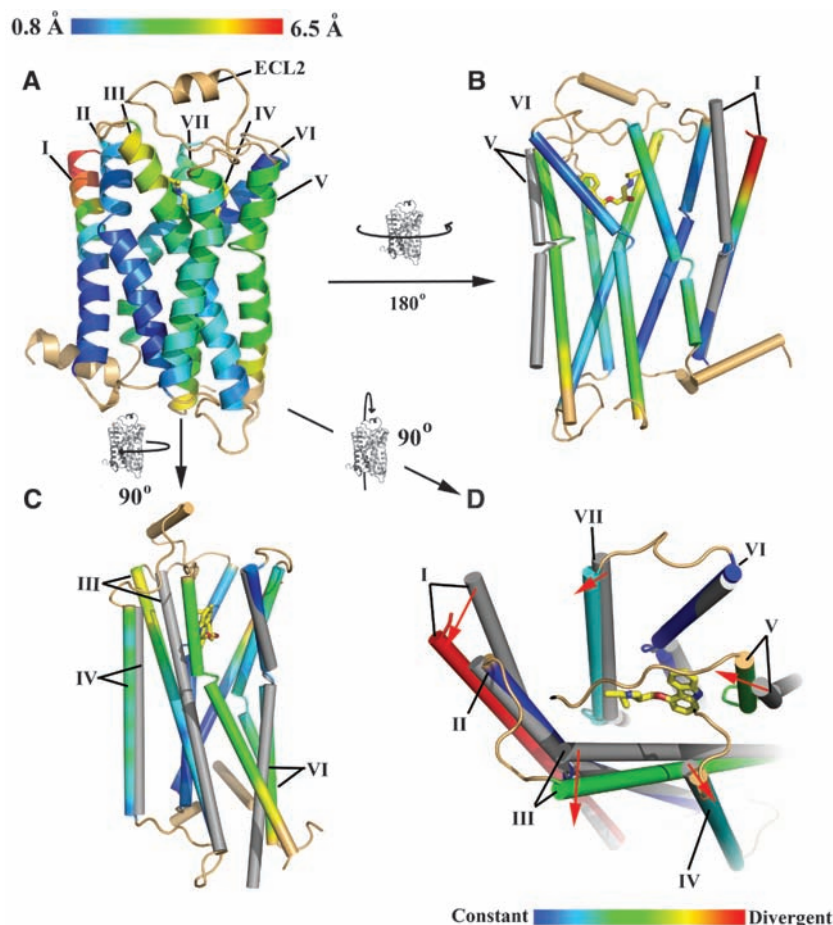
Fig. 6. Comparison of β_2AR-T4L helical orientations with those of rhodopsin (PDB ID code 1U19). (**A**) β_2AR-T4L is rendered as a ribbon trace colored with a blue-to-red spectrum corresponding to observed distances between Cα positions in the two structures [root mean square deviation (RMSD) 2.7 Å between all residues in the transmembrane region]. Helix II shows very little movement, whereas the entire lengths of helices III, IV, and V shift substantially. Helix VIII and loops were not included in the comparison and are colored tan. (**B**) Movements of helices I and V of rhodopsin (gray) are shown relative to β_2AR-T4L. (**C**) Movements of helices III, IV, and VI. (**D**) Ligand-binding site representation. Carazolol is shown with yellow carbons. Entire helices are assigned a single designation on the basis of their divergence from the rhodopsin position in the area of the ligand-binding site as shown. Helix I is highly divergent; helices II and VI are similar to rhodopsin. Helices IV and VII are moderately constant. Helices III and V are moderately divergent.

References and Notes
1. S. Takeda, S. Kadowaki, T. Haga, H. Takaesu, S. Mitaku, *FEBS Lett.* **520**, 97 (2002).
2. R. Fredriksson, M. C. Lagerstrom, L. G. Lundin, H. B. Schioth, *Mol. Pharmacol.* **63**, 1256 (2003).
3. K. L. Pierce, R. T. Premont, R. J. Lefkowitz, *Nat. Rev. Mol. Cell Biol.* **3**, 639 (2002).
4. R. J. Lefkowitz, S. K. Shenoy, *Science* **308**, 512 (2005).
5. Y. Sun *et al.*, *EMBO J.* **26**, 53 (2007).
6. J. Drews, *Science* **287**, 1960 (2000).
7. B. Kobilka, *Annu. Rev. Neurosci.* **15**, 87 (1992).

8. M. G. Caron, R. J. Lefkowitz, *Recent Prog. Horm. Res.* **48**, 277 (1993).
9. A. D. Strosberg, *Protein Sci.* **2**, 1198 (1993).
10. L. Hein, B. K. Kobilka, *Trends Cardiovasc. Med.* **7**, 137 (1997).
11. D. K. Rohrer, *J. Mol. Med.* **76**, 764 (1998).
12. Y. Xiang, B. Kobilka, in *The Adrenergic Receptors in the 21st Century*, D. M. Perez, Ed. (Humana, Totowa, NJ, 2006), pp. 267–292.
13. G. Milligan, P. Svoboda, C. M. Brown, *Biochem. Pharmacol.* **48**, 1059 (1994).
14. M. R. Taylor, *Pharmacogenomics J.* **7**, 29 (2007).
15. T. R. Bai, *Lung* **170**, 125 (1992).
16. P. J. Barnes, *Life Sci.* **52**, 2101 (1993).
17. R. M. Smiley, M. Finster, *J. Matern. Fetal Med.* **5**, 106 (1996).
18. K. Palczewski *et al.*, *Science* **289**, 739 (2000).
19. T. Okada *et al.*, *J. Mol. Biol.* **342**, 571 (2004).
20. J. Li, P. C. Edwards, M. Burghammer, C. Villa, G. F. Schertler, *J. Mol. Biol.* **343**, 1409 (2004).
21. D. Salom *et al.*, *Proc. Natl. Acad. Sci. U.S.A.* **103**, 16123 (2006).
22. B. K. Kobilka, X. Deupi, *Trends Pharmacol. Sci.* **28**, 397 (2007).
23. Inverse agonists act to reduce the basal activity of a receptor through interactions that shift the equilibrium to more of an inactive state. In contrast, antagonists bind to and block the active site but do not affect the equilibrium between inactive and active states, and agonists shift the equilibrium to an active receptor state.
24. D. M. Rosenbaum *et al.*, *Science* **318**, 1266; published online 25 October 2007 (10.1126/science.1150609).
25. β_2AR-T4L was generated by three distinct modifications to β_2AR: (i) a fusion protein was created by replacement of the third intracellular loop with T4L, (ii) the C-terminal 48 amino acids were deleted, and (iii) a glycosylation site at Asn[187] was eliminated through a Glu substitution. This modified version was created to assist in improved crystal formation.
26. E. M. Landau, E. Pebay-Peyroula, R. Neutze, *FEBS Lett.* **555**, 51 (2003).
27. See supporting material on *Science* Online.
28. M. Caffrey, *Curr. Opin. Struct. Biol.* **10**, 486 (2000).
29. J. Deisenhofer, H. Michel, *EMBO J.* **8**, 2149 (1989).
30. E. M. Landau, J. P. Rosenbusch, *Proc. Natl. Acad. Sci. U.S.A.* **93**, 14532 (1996).
31. Z. Yao, B. Kobilka, *Anal. Biochem.* **343**, 344 (2005).
32. V. Cherezov, A. Peddi, L. Muthusubramaniam, Y. F. Zheng, M. Caffrey, *Acta Crystallogr. D* **60**, 1795 (2004).
33. The successful diffraction screening and data collection that led to the structure determination of β_2AR-T4L required overcoming a number of technological barriers that encompassed the growth and harvest of microcrystals, crystal imaging, and collection of diffraction data. Because of their transparency, crystals were often visually obstructed by the frozen lipidic mesophase material and therefore could not be confidently imaged by traditional beamline cameras; moreover, their extremely small size made them susceptible to rapid radiation damage (*27*).
34. GPCRs are frequently posttranslationally modified with palmitoylate on cysteine residues at the C-terminal tail. Furthermore, β_2AR-T4L was treated with iodoacetamide during purification to eliminate free thiols.
35. In Ballesteros-Weinstein numbering, a single most conserved residue among the class A GPCRs is designated x.50, where x is the transmembrane helix number. All other residues on that helix are numbered relative to this conserved position.
36. S. Yohannan, S. Faham, D. Yang, J. P. Whitelegge, J. U. Bowie, *Proc. Natl. Acad. Sci. U.S.A.* **101**, 959 (2004).
37. M. Katragadda, M. W. Maciejewski, P. L. Yeagle, *Biochim. Biophys. Acta* **1663**, 74 (2004).
38. V. Cherezov *et al*, *J. Mol. Biol.* **364**, 716 (2006).
39. Membrane proteins generally can form two types of crystal packing. Type I represents stacks of two-dimensional crystals ordered in the third dimension via interactions of hydrophilic parts of membrane proteins. Type II crystals are composed of membrane proteins whose hydrophobic part is shielded by a detergent micelle, and all crystal contacts are formed through hydrophilic, solvent-exposed parts of protein molecules.
40. P. Nollert, H. Qiu, M. Caffrey, J. P. Rosenbusch, E. M. Landau, *FEBS Lett.* **504**, 179 (2001).
41. B. F. O'Dowd, M. Hnatowich, M. G. Caron, R. J. Lefkowitz, M. Bouvier, *J. Biol. Chem.* **264**, 7564 (1989).
42. G. Milligan, *Mol. Pharmacol.* **66**, 1 (2004).
43. S. Angers *et al.*, *Proc. Natl. Acad. Sci. U.S.A.* **97**, 3684 (2000).
44. J. A. Javitch, *Mol. Pharmacol.* **66**, 1077 (2004).
45. J. F. Mercier, A. Salahpour, S. Angers, A. Breit, M. Bouvier, *J. Biol. Chem.* **277**, 44925 (2002).
46. G. F. Schertler, *Curr. Opin. Struct. Biol.* **15**, 408 (2005).
47. T. E. Hebert *et al.*, *J. Biol. Chem.* **271**, 16384 (1996).
48. W. Guo, L. Shi, J. A. Javitch, *J. Biol. Chem.* **278**, 4385 (2003).
49. Y. Xiang, V. O. Rybin, S. F. Steinberg, B. Kobilka, *J. Biol. Chem.* **277**, 34280 (2002).
50. M. R. Whorton *et al.*, *Proc. Natl. Acad. Sci. U.S.A.* **104**, 7682 (2007).
51. R. S. Ostrom, P. A. Insel, *Br. J. Pharmacol.* **143**, 235 (2004).
52. N. A. Baker, D. Sept, S. Joseph, M. J. Holst, J. A. McCammon, *Proc. Natl. Acad. Sci. U.S.A.* **98**, 10037 (2001).
53. T. H. Ji, M. Grossmann, I. Ji, *J. Biol. Chem.* **273**, 17299 (1998).
54. U. Gether, *Endocr. Rev.* **21**, 90 (2000).
55. K. Noda, Y. Saad, R. M. Graham, S. S. Karnik, *J. Biol. Chem.* **269**, 6743 (1994).
56. J. Mialet-Perez, S. A. Green, W. E. Miller, S. B. Liggett, *J. Biol. Chem.* **279**, 38603 (2004).
57. S. G. F. Rasmussen *et al.*, *Nature*, published online 21 October 2007 (10.1038/nature06325).
58. K. Palczewski, *Annu. Rev. Biochem.* **75**, 743 (2006).
59. T. W. Schwartz, T. M. Frimurer, B. Holst, M. M. Rosenkilde, C. E. Elling, *Annu. Rev. Pharmacol. Toxicol.* **46**, 481 (2006).
60. L. Shi *et al.*, *J. Biol. Chem.* **277**, 40989 (2002).
61. R. J. Lefkowitz, *Nat. Cell Biol.* **2**, E133 (2000).
62. For the alignment, residues on β_2AR were aligned to equivalent residues on rhodopsin: Residues 43 to 59 were aligned to residues 47 to 63; residues 67 to 95 were aligned to residues 71 to 99; residues 122 to 135 were aligned to residues 126 to 139; and residues 285 to 296 were aligned to residues 264 to 275.
63. C. D. Strader *et al.*, *J. Biol. Chem.* **263**, 10267 (1988).
64. C. D. Strader, M. R. Candelore, W. S. Hill, I. S. Sigal, R. A. Dixon, *J. Biol. Chem.* **264**, 13572 (1989).
65. G. Liapakis *et al.*, *J. Biol. Chem.* **275**, 37779 (2000).
66. C. Bissantz, P. Bernard, M. Hibert, D. Rognan, *Proteins* **50**, 5 (2003).
67. A. Fano, D. W. Ritchie, A. Carrieri, *J. Chem. Inf. Model.* **46**, 1223 (2006).
68. J. V. Hobrath, S. Wang, *J. Med. Chem.* **49**, 4470 (2006).
69. M. Nowak, M. Kolaczkowski, M. Pawlowski, A. J. Bojarski, *J. Med. Chem.* **49**, 205 (2006).
70. Y. Zhang, M. E. Devries, J. Skolnick, *PLoS Comput. Biol.* **2**, e13 (2006).
71. P. L. Freddolino *et al.*, *Proc. Natl. Acad. Sci. U.S.A.* **101**, 2736 (2004).
72. K. E. Furse, T. P. Lybrand, *J. Med. Chem.* **46**, 4450 (2003).
73. P. R. Gouldson *et al.*, *Proteins* **56**, 67 (2004).
74. M. A. Lomize, A. L. Lomize, I. D. Pogozheva, H. I. Mosberg, *Bioinformatics* **22**, 623 (2006).
75. W. L. DeLano, The PyMOL Molecular Graphics System (2002) (www.pymol.org).

Supporting Online Material